Biophysical Journal, Volume 96

Supporting Material

Microscopic mechanism for experimentally observed anomalous elasticity of DNA in 2D

Nicolas Destainville, Manoel Manghi, and John Palmeri

Supplementary Information to the paper "Microscopic mechanism for experimentally observed anomalous elasticity of DNA in 2D"

N. Destainville, M. Manghi, J. Palmeri

Université de Toulouse; UPS; Laboratoire de Physique Théorique (IRSAMC); F-31062 Toulouse, France
CNRS; LPT (IRSAMC); F-31062 Toulouse, France

January 28, 2009

A. Effective Ising Hamiltonian

Starting from the Hamiltonian $H[\sigma_i, \mathbf{t}_i]$, an effective Ising Hamiltonian, a function of the σ_i only, is obtained by integrating out the rotational degrees of freedom $\mathbf{t}_i$ in the partition function, leading to a renormalized Hamiltonian,

$$H_0[\sigma_i] \;=\; -\sum_{i=1}^{N-1}\left[J_0\sigma_{i+1}\sigma_i + \frac{K_0}{2}(\sigma_{i+1}+\sigma_i)\right] - \mu\sum_{i=1}^{N}\sigma_i, \tag{1}$$

with renormalized parameters: $J_0 = J - k_BT[G_0(\beta\kappa_U) + G_0(\beta\kappa_B) - 2G_0(\beta\kappa_{UB})]/4$ and $K_0 = -k_BT[G_0(\beta\kappa_U) - G_0(\beta\kappa_B)]/2$ where $\beta = (k_BT)^{-1}$ and $G_0(x) = x - \ln(\sinh x/x)$ is related to the bending free energy of a single joint; μ is not renormalized (see Ref. [1] for further details).

B. Calculations of the probability distribution $p(\cos\theta)$ in 3D

In Eq. (3) of the body of the text, we define the partial partition function where all degrees of freedom are integrated out, except the projections on the z axis of $\mathbf{t}_i$ and $\mathbf{t}_{i+r}$, set respectively to z_i and z_{i+r}. Imposing the value of $\mathbf{t}_i\cdot\mathbf{t}_{i+r} \equiv s \in [-1,1]$ amounts to fixing $z_i = 1$ (i.e. $\mathbf{t}_i = \mathbf{z}$), and $z_{i+r} = s$ (see Fig.SI. 1) and to multiplying by the solid angle 4π to restore the rotational invariance of the whole problem with respect to $\mathbf{t}_i$, which can actually take any orientation. Thus we have $p(\mathbf{t}_i\cdot\mathbf{t}_{i+r} = s) = 4\pi Z(1,s)/Z$ where

$$Z = \langle V|\hat{P}^{N-1}|V\rangle \tag{2}$$

is the total partition function (see Methods and Ref. [1]).

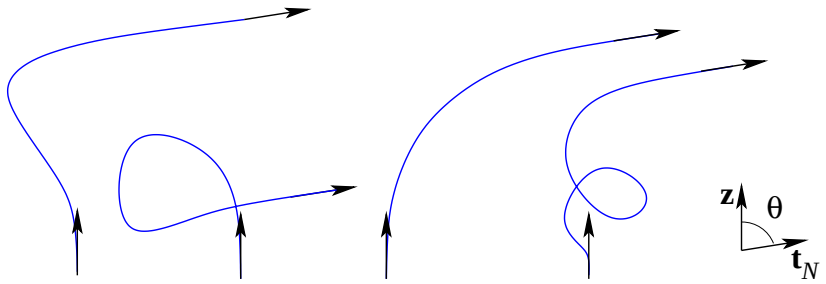

Fig.SI. 1: Examples of chain configurations counted by the same partial partition function $Z(1,s)$ (Eq. (3) of the body of the text), in the case where the singled-out tangent vectors lie on the polymer ends, $\mathbf{t}_i = \mathbf{t}_1 = \mathbf{z}$, $\mathbf{t}_{i+r} = \mathbf{t}_N$ and $s = \mathbf{z}\cdot\mathbf{t}_N = \cos\theta$.

We denote by $\hat{\Pi}_z$ the projector on the z axis defined by $\hat{\Pi}_z|\sigma\Omega\rangle = \delta(\cos\theta - z)|\sigma\Omega\rangle$. It follows from Eq. (3) of the body of the text that

$$Z(z_i, z_{i+r}) = \langle V|\hat{P}^{i-1}\hat{\Pi}_{z_i}\hat{P}^{r}\hat{\Pi}_{z_{i+r}}\hat{P}^{N-r-i}|V\rangle. \tag{3}$$

In order to compute this quantity, we need to express $\hat{\Pi}_z$ in the basis where $\hat{P}$ is diagonal, namely the $|\hat{\Psi}_{l,m;\tau}\rangle$. We use

$$\langle\sigma\Omega|\hat{\Psi}_{l,m;\tau}\rangle = \psi_{l,m}(\Omega)\langle\sigma|l,\tau\rangle, \tag{4}$$

where the spherical harmonics $\psi_{l,m}$ are defined by the Associated Legendre polynomials $P_{l,m}$ [2] as follows:

$$\psi_{l,m}(\Omega) \equiv \psi_{l,m}(\theta,\varphi) = k_{l,m}P_{l,|m|}(\cos\theta)e^{im\varphi}, \tag{5}$$

$$k_{l,m} = \sqrt{(2l+1)\frac{(l-|m|)!}{(l+|m|)!}}. \tag{6}$$

Below, we shall only need the Legendre polynomials $P_l(x) \equiv P_{l,m=0}(x)$ [2]. Now we can compute

$$\langle\hat{\Psi}_{l',m';\tau'}|\hat{\Pi}_z|\hat{\Psi}_{l,m;\tau}\rangle = \sum_{\sigma=\pm}\int\frac{d\Omega}{4\pi}\langle\hat{\Psi}_{l',m';\tau'}|\hat{\Pi}_z|\sigma\Omega\rangle\langle\sigma\Omega|\hat{\Psi}_{l,m;\tau}\rangle \tag{7}$$

$$= \sum_{\sigma=\pm}\int\frac{d\Omega}{4\pi}\langle\hat{\Psi}_{l',m';\tau'}|\sigma\Omega\rangle\delta(\cos\theta - z)\langle\sigma\Omega|\hat{\Psi}_{l,m;\tau}\rangle \tag{8}$$

$$= \frac{1}{4\pi}k_{l,m}k_{l',m'}\sum_{\sigma=\pm}\int_0^{2\pi}d\varphi P_{l,|m|}(z)P_{l',|m'|}(z)e^{i(m-m')\varphi}\langle l',\tau'|\sigma\rangle\langle\sigma|l,\tau\rangle \tag{9}$$

$$= \frac{1}{2}k_{l,m}k_{l',m}P_{l,|m|}(z)P_{l',|m|}(z)\langle l',\tau'|l,\tau\rangle\delta_{m,m'}. \tag{10}$$

When $m = m' = 0$, the previous equality specializes to

$$\langle\hat{\Psi}_{l',0;\tau'}|\hat{\Pi}_z|\hat{\Psi}_{l,0;\tau}\rangle = \frac{1}{2}\sqrt{2l+1}\sqrt{2l'+1}P_l(z)P_{l'}(z)\langle l',\tau'|l,\tau\rangle. \tag{11}$$

If the boundary vector $|V\rangle$ has rotational symmetry ($l = 0$), then $\langle\hat{\Psi}_{l,m;\tau}|V\rangle = \delta_{l0}\delta_{m0}\langle 0,\tau|V\rangle$. It follows that

$$4\pi Z(z_i, z_{i+r}) = \sum_{\{\tau,\tau',\tau''\}}\sum_{l=0}^{\infty}\frac{2l+1}{2}\langle V|0,\tau\rangle\lambda_{0,\tau}^{i-1}P_0(z_i)\langle 0,\tau|l,\tau'\rangle P_l(z_i)\lambda_{l,\tau'}^r P_l(z_{i+r})\langle l,\tau'|0,\tau''\rangle P_0(z_{i+r})\lambda_{0,\tau''}^{N-r-i}\langle 0,\tau''|V\rangle. \tag{12}$$

This partial partition function must be compared to the complete one

$$Z = \langle V|\,\hat{P}^{N-1}\,|V\rangle = \sum_\tau |\langle V|0,\tau\rangle|^2\lambda_{0,\tau}^{N-1} \tag{13}$$

in order to get

$$p(\mathbf{t}_i\cdot\mathbf{t}_{i+r} = s) = \frac{\sum_{\{\tau,\tau',\tau''\}}\sum_{l=0}^{\infty}(2l+1)\langle V|0,\tau\rangle\lambda_{0,\tau}^{i-1}\langle 0,\tau|l,\tau'\rangle\lambda_{l,\tau'}^r P_l(s)\langle l,\tau'|0,\tau''\rangle\lambda_{0,\tau''}^{N-r-i}\langle 0,\tau''|V\rangle}{2\sum_\tau|\langle V|0,\tau\rangle|^2\lambda_{0,\tau}^{N-1}} \tag{14}$$

because $P_0(1) = P_0(z) = P_l(1) = 1$. One can check that the distribution is correctly normalized, $\int_{-1}^1 p(s)\,ds = 1$, because $\int_{-1}^1 P_l(s)\,ds = 2\delta_{l,0}$.

In the limit of a long DNA where the internal segment $[i, i+r]$ is far from both chain ends, in other words when $N\to\infty$ and then $i\to\infty$, the previous relation becomes

$$p(\mathbf{t}_i\cdot\mathbf{t}_{i+r} = s) = \sum_{l=0}^{\infty}\frac{2l+1}{2}P_l(s)\sum_{\tau'=\pm}|\langle 0,+|l,\tau'\rangle|^2\left(\frac{\lambda_{l,\tau'}}{\lambda_{0,+}}\right)^r \tag{15}$$

$$= \frac{1}{2} + \sum_{l=1}^{\infty}\frac{2l+1}{2}P_l(s)\sum_{\tau'=\pm}|\langle 0,+|l,\tau'\rangle|^2 e^{-r/\xi^p_{l,\tau}}. \tag{16}$$

This expression reveals the role of infinitely many correlation lengths, the $\xi^p_{l,\tau} = 1/\ln(\lambda_{0,+}/\lambda_{l,\tau})$. At T_R, the persistence length $\xi^p \simeq 150$ bp coincides with $\xi^p_{1,+}$ [1, 3]. We have checked that boundary effects are indeed negligible at

room temperature ($T_R = 298.15$ K) as soon as i is larger than a few unities. Thus Eq. (16) is a sufficient approximation of Eq. (14) for fitting purposes and is used in the body of the text. Once this distribution $p(\cos\theta)$ is known, the probability distribution of θ, denoted by $\tilde{p}(\theta)$, is simply given by $\tilde{p}(\theta) = p(\cos\theta)\sin\theta \mathrm{d}\theta$, because $s = \cos\theta$ and $|ds| = \sin\theta\ |d\theta|$.

As a corollary, the mean value of the correlator $\langle \mathbf{t}_i \cdot \mathbf{t}_{i+r} \rangle$ can be computed in this limit:

$$\langle \mathbf{t}_i \cdot \mathbf{t}_{i+r} \rangle = \int_{-1}^{1} s\ p(s)\ ds \tag{17}$$

$$= \sum_{l=0}^{\infty} \frac{2l+1}{2} \left(\int_{-1}^{1} s\ P_l(s)\ ds \right) \sum_{\tau'=\pm} |\langle 0,+|l,\tau'\rangle|^2 \left(\frac{\lambda_{l,\tau'}}{\lambda_{0,+}} \right)^r \tag{18}$$

$$= \sum_{\tau'=\pm} |\langle 0,+|1,\tau'\rangle|^2 \left(\frac{\lambda_{1,\tau'}}{\lambda_{0,+}} \right)^r, \tag{19}$$

because $\int_{-1}^{1} s\ P_l(s)\ ds = \frac{2}{3}\delta_{l,1}$. We therefore recover the result of Ref. [1], Eq. (100), where it is pointed out that only two correlation lengths remain in this correlator.

C. Calculations of $p(\theta)$ in 2D

Using the 2D algebraic background presented in the Methods and the fact that $\langle \sigma\theta|\hat{\Psi}_{n;\tau}\rangle = e^{in\theta}\langle\sigma|n,\tau\rangle$, the matrix elements of the projectors $\hat{\Pi}_z$ in the eigenbasis become

$$\langle \hat{\Psi}_{n';\tau'}|\hat{\Pi}_z|\hat{\Psi}_{n;\tau}\rangle = \sum_{\sigma=\pm} \int_{-\pi}^{\pi} \frac{d\theta}{2\pi} \langle \hat{\Psi}_{n';\tau'}|\sigma\theta\rangle \delta(\theta-\theta_0) \langle\sigma\theta|\hat{\Psi}_{n;\tau}\rangle \tag{20}$$

$$= \frac{1}{2\pi} \sum_{\sigma=\pm} e^{i(n-n')\theta_0} \langle n',\tau'|\sigma\rangle\langle\sigma|n,\tau\rangle \tag{21}$$

$$= \frac{1}{2\pi} e^{i(n-n')\theta_0} \langle n',\tau'|n,\tau\rangle. \tag{22}$$

In addition, $\langle \hat{\Psi}_{n;\tau}|V\rangle = \delta_{n0}\langle 0,\tau|V\rangle$ by the rotational symmetry of the boundary conditions, and comparing the partial partition function, now denoted by $Z(\theta)$, with the full one, Z, leads to the 2D counterpart of Eq. (16):

$$p(\theta_r = \theta) = \frac{Z(\theta)}{Z} \tag{23}$$

$$= \frac{1}{2\pi} \sum_{n=-\infty}^{\infty} \cos(n\theta) \sum_{\tau'=\pm} |\langle 0,+|n,\tau'\rangle|^2 \left(\frac{\lambda_{n,\tau'}}{\lambda_{0,+}} \right)^r \tag{24}$$

$$= \frac{1}{2\pi} + \frac{1}{\pi} \sum_{n=1}^{\infty} \cos(n\theta) \sum_{\tau=\pm} \langle 0,+|n,\tau\rangle^2\, e^{-r/\xi^p_{n,\tau}}, \tag{25}$$

valid in the limit of long DNA strands, with $\theta_r \in (-\pi,\pi]$ defined by $\cos\theta_r \equiv \mathbf{t}_i \cdot \mathbf{t}_{i+r}$ and $\xi^p_{n,\tau} \equiv 1/\ln(\lambda_{0,+}/\lambda_{n,\tau})$.

D. Fitting $p(\theta)$ in 2D

Our first approach to fitting the 2D experimental data of Fig. 2B of the body of the text, coming from Ref. [4], consisted in directly using the 3D parameter values, in particular those of J and μ, in the 2D Hamiltonian. The so-obtained angle probabilities are very far from the experimental ones, which led us to fit the model to experiment.

We display in Fig. 2B of the body of the text our best model fits, using Eq. (25) with κ_{UB}, J and μ, as fitting parameters. These least-square fits are good over the whole θ range. The bp length is assumed to remain $a = 0.34$ nm. Thus the curvilinear distances between monomers in [4], namely 5, 10 and 30 nm, correspond respectively to $r = 15$, 29 and 88 bp. The value (in units of k_BT_R) of $\kappa_B = 5.54$ comes from Ref. [3] and $\kappa_U = 160.82$ comes from fitting the $r = 88$ bp set of data by a pure WLC model, as in [4] (assuming that for such a large r, the Gaussian character

is restored thanks to the central-limit theorem; we have checked that it is indeed the case for the parameters that we discuss now). The three remaining parameters (κ_{UB}, J, μ) are fitted by a simulated annealing algorithm of our own. The best fit values appear to be highly degenerate, in the sense that a whole subset of parameters in the three-dimensional (κ_{UB}, J, μ) space yields essentially the same mean-square deviation.

This degeneracy can be related to its 3D equivalent. In Ref. [1], we have simplified the discussion by setting $\kappa_{UB} = \kappa_U$, the value for dsDNA, because varying κ_{UB} amounts simply to changing the bare value of J in order to keep the melting temperature, T_m, and the transition width unchanged: $J_{\rm mod} = J + \frac{k_B T}{2}[G_0(\beta\kappa_U) - G_0(\beta\kappa_{UB})]$ [1]. However, when it comes to the angle distribution p, the value of κ_{UB} might play a more fundamental role because the different persistence lengths depend on it *via* the eigenvalues λ in Eq. (25). In 3D, we have checked that changing the value of κ_{UB}, while suitably modifying J, has, in practice, little influence on p, N_r, and ΔM_B (see definitions below), even at very short scales ($r = 5$ bp). In 2D, suitable values of κ_{UB} range between 10 and 50 $k_B T_R$. Even if $\kappa_{UB} = \kappa_U$ or $\kappa_{UB} = \kappa_B$ is held fixed, the minimization with respect to J and μ alone does not give a significantly poorer fit. Examples of parameter sets provided by simulated annealing are, in units of $k_B T_R$, (κ_{UB}, J, μ) =(20.97,1.3173,1.6685) or (45.10,0.8637,1.7885). Increasing the temperature by 20% does not lift the degeneracy. With these values, the fraction of melted bps for an unconstrained DNA varies between $\varphi_B = 0.1\%$ and 0.4% at T_R.

E. Probability distribution $p(\theta)$ calculated from diverse Hamiltonians in 2D discussed in the paper

We consider a pure elastic chain without bp melting, described by a 2D single-joint Hamiltonian $H(\theta)$. Without any loss of generality, the probability distribution $p(\theta)$ in 2D can be written as

$$p(\theta) = \frac{\prod_{i=1}^{r} \int_{-\pi}^{\pi} d\theta_i \, \exp\left[-\beta H(\theta_i)\right] \, \delta(\theta - \theta_{i,i+r})}{\prod_{i=1}^{r} \int_{-\pi}^{\pi} d\theta_i \, \exp\left[-\beta H(\theta_i)\right]} \tag{26}$$

where $\theta \equiv \theta_{i,i+r} = \sum_{j=1}^{i+r-1} \theta_j$ is the bending angle between $\mathbf{t}_i$ and $\mathbf{t}_{i+r}$. By introducing the Fourier transform of the δ distribution, we get

$$p(\theta) = \frac{1}{2\pi} \int_{-\infty}^{\infty} d\omega \, e^{i\omega\theta} \left[\frac{z(\omega)}{z(0)}\right]^r \tag{27}$$

where the characteristic function of the single-joint Hamiltonian is defined by

$$z(\omega) = \int_{-\pi}^{\pi} d\theta \, \exp\left[-i\omega\theta - \beta H(\theta)\right]. \tag{28}$$

We consider four cases:

1. For a Gaussian Hamiltonian (Gaussian Spin Wave approximation, GSW), $H(\theta) = \kappa\theta^2/2$ with the approximation $\theta \in (-\infty, \infty)$, we have $z(\omega)/z(0) = \exp[-\omega^2/(2\beta\kappa)]$ and we easily get the Gaussian probability distribution in 2D

$$p_{\rm GSW}(\theta) = \sqrt{\frac{\beta\kappa}{2\pi r}} \, \exp\left(-\frac{\beta\kappa\theta^2}{2r}\right). \tag{29}$$

2. For the discrete wormlike chain where $H(\theta) = \kappa(1 - \cos\theta)$ is periodic in $\theta \in (-\pi, \pi]$, Eq.(27) reduces to a decomposition in Fourier series of modes n with $z(\omega)$ becoming $e^{-\beta\kappa} I_n(\beta\kappa)$ and we find

$$p_{\rm DWLC}(\theta) = \frac{1}{2\pi} \sum_{n=-\infty}^{\infty} \cos(n\theta) \left[\frac{I_n(\beta\kappa)}{I_0(\beta\kappa)}\right]^r. \tag{30}$$

   This is equivalent to Eq. (25) in the simple case where all the κ are set equal.

3. For the LSEC model [4, 5], where $H(\theta) = \Lambda|\theta|$ with the approximation $\theta \in (-\infty, \infty)$, we have $z(\omega)/z(0) = 1/[1 + (\omega/\beta\Lambda)^2]$ and the probability distribution is

$$p_{\rm LSEC}(\theta) = \frac{2^{\frac{1}{2}-r}\beta\Lambda}{\sqrt{\pi}} \frac{(\beta\Lambda|\theta|)^{r-\frac{1}{2}} K_{\frac{1}{2}-r}(\beta\Lambda|\theta|)}{\Gamma(r)}, \tag{31}$$

   where Γ is the Euler function and $K_\nu(x)$ the modified Hankel function [2]. Equation (31) is plotted for different temperature values in Fig. 3 of the body of the text. Note that in the case where $\theta \in (-\pi, \pi]$, the above result has a negligible correction to p on the order of $\exp(-\beta\Lambda\pi) \simeq 5 \times 10^{-10}$ rad^{-1} if $\beta\Lambda \simeq 6.8$ [4].

4. Both the GSW and LSEC models are special cases of a generalized model where $H(\theta) = \alpha|\theta|^\eta$. With the approximation $\theta \in (-\infty, \infty)$, we recover the GSW model when $\eta = 2$, $\alpha = \kappa/2$ and the LSEC model when $\eta = 1$, $\alpha = \Lambda$. Although the general case is harder to handle for arbitrary r, two limits, $r = 1$ and large r, are easily studied. When $r = 1$,

$$p(\theta) = \frac{\exp[-\beta H(\theta)]}{\int_{-\infty}^{+\infty} d\theta' \exp[-\beta H(\theta')]} = \frac{\eta(\beta\alpha)^{1/\eta}}{2\Gamma(1/\eta)} \exp[-\beta\alpha|\theta|^\eta], \qquad (r = 1). \tag{32}$$

For large r, $[z(\omega)/z(0)]^r$ becomes a sharply peaked Gaussian function centered at $\omega = 0$: $[z(\omega)/z(0)]^r \simeq \exp[-r\omega^2\langle\theta^2\rangle/2]$. In this limit $p(\theta)$ becomes effectively Gaussian,

$$p(\theta) \simeq \sqrt{\frac{\beta\kappa_{\rm eff}}{2\pi r}} \exp\left(-\frac{\beta\kappa_{\rm eff}\theta^2}{2r}\right), \qquad \text{(large r)}, \tag{33}$$

where $\kappa_{\rm eff}(\alpha, \eta; \beta) \equiv 1/(\beta\langle\theta^2\rangle) = (\beta\alpha)^{2/\eta}\Gamma(1/\eta)/[\beta\Gamma(3/\eta)]$. The effective bending rigidity, $\kappa_{\rm eff} = (\xi/\ell)\beta^{-1}$, can be written in terms of the asymptotic persistence length, ξ, the segment length, ℓ, and the temperature. It is only for $\eta = 2$ that $p(\theta)$ is Gaussian at all length scales r. For strongly subharmonic models (η well below 2), the large angle bending distribution can be much higher than the Gaussian model prediction for $r \ll \xi$ (see Fig. 3A of Wiggins et al. [4] for the $\eta = 1$ case). For non-Gaussian models, $p(\theta)$ interpolates smoothly between an "anomalous" behavior [Eq. (32)] and an effective Gaussian one [Eq. (33)] as r increases from one past the persistence length, ξ. For large r, even at large θ, $p(\theta)$ is effectively Gaussian because it is determined mainly by those high entropy configurations for which almost all joint angles, θ_j, are small (therefore in this case only the small θ behavior of $H(\theta)$ is important).

From fitting the large r data to the Gaussian model, Wiggins et al. found $\beta\kappa_{\rm eff} = \xi/\ell = 54\,{\rm nm}/2.5\,{\rm nm} \simeq 22$, which implies that $\beta\Lambda = \beta\alpha_{\rm LSEC} = (2\beta\kappa_{\rm eff})^{1/2} = 6.6$, close to the value of 6.8 found by fitting their LSEC model to experiment using Monte Carlo simulations.

F. Bending-induced melting in 2D

Following Wiggins *et al.* [6], we now derive the average bending moment N_r as a function of the deflection angle θ. In the 2D case,

$$N_r \equiv \frac{\partial}{\partial\theta} \ln Z(\theta) \tag{34}$$

(in units of k_BT) measures the torque perpendicular to the substrate that must be applied to two interior monomers separated by r bp in order to impose a deflection angle θ between them. Examples of N_r vs θ plots for our model are given in Fig.SI. 2. Four regimes appear in these plots:

(i) a linear one at low deflection angle $\theta < \theta_c$;

(ii) a non-linear one for intermediate angles;

(iii) a saturation plateau for large deflection angles and

(iv) a decreasing one near $\theta = \pi$.

In regime (i), the DNA response is linear, with a GSW bending moment $N_r = \beta\partial F(\theta, r)/\partial\theta = (\xi^p/r)\theta$, determined only by $\xi^p \simeq \beta\kappa_U$, since melted bps are essentially inexistent. In the intermediate region (ii), a non-linear behavior occurs. Indeed, it becomes more favorable for the system to break bps in order to make them more flexible and thereby relax the high bending constraint. The plateau appearing in region (iii) shows non-zero response due to the finite value of κ_B, contrary to the kink model [6]. As already mentioned in this Ref. [6], when θ approaches π [regime (iv)], N_r vanishes: the symmetry of the system through the axis defined by the vectors $\mathbf{t}_i$ and $\mathbf{t}_{i+r}$ imposes that $\theta = \pi$ is an (unstable) equilibrium point. Indeed, $\theta \in (-\pi, \pi]$ in our calculations, thus larger angles are brought back in this interval modulo 2π. For a given θ, the summation in Z is in fact a sum over all the $\theta + 2k\pi$, $k \in \mathbb{Z}$, as illustrated in Fig.SI. 1. Since the contributions of $\theta = \pi$ and $\theta = -\pi$ cancel, N_r vanishes at $\theta = \pi$. More importantly, we cannot give quantitative answers for cyclization experiments when $|\theta| \approx 2\pi$.

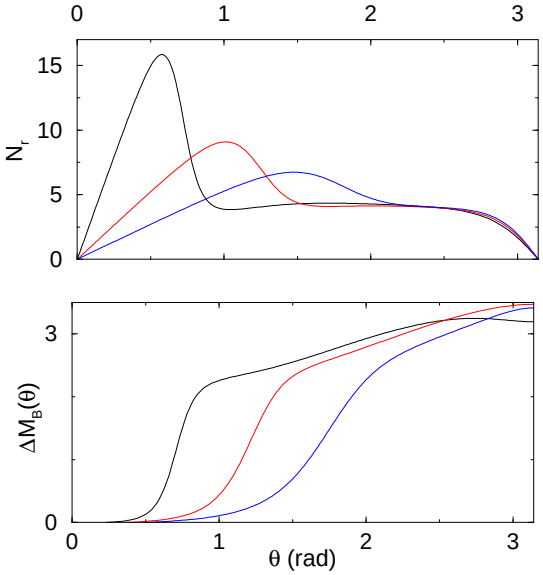

Fig.SI. 2: Torque N_r (top) and excess chain melting ΔM_B (bottom) as a function of θ, in 2D. Same parameter values as in Fig. 2B of the body of the text. From left to right, $r = 5, 15, 25$ bp. The elasticity is linear until a threshold $\theta_c \propto \sqrt{r}$, where excessive bending induces bp melting.

To render these physical mechanisms more explicit, we have also displayed in Fig.SI. 2 the excess chain melting ΔM_B as a function of θ (Fig. 2D in the body of the text). It measures the average excess of melted bps in the bended chain as compared to the free, unconstrained one and is given by $\Delta M_B \equiv -\frac{k_B T}{2}\frac{\partial}{\partial \mu} \ln p(\theta)$. We thus confirm that the collapse of N_r corresponds to the proliferation of melted bps. The typical angle θ_c at which bending-induced melting occurs is again estimated by equating the energetic cost of bending the polymer in its unmelted state, of order $\beta \kappa_U \theta_c^2/2r$, with the free-energy cost of nucleating a single denaturation bubble (of one bp), $\Delta G_B = 4J_0 + 2K_0 + 2\mu$ [1]. Again, this argument that leads to $\theta_c \sim \sqrt{r}$ gives a good estimate of the observed threshold. It also gives the upper limit of r for which these non-linearities are apparent, $r_{\max} \approx \frac{\pi^2}{2}\kappa_U/\Delta G_B \simeq 120$ bp in 2D.

An interesting feature of these calculations is the saturation of ΔM_B at a finite value [regions (iii) and (iv)], even when $r < r_{\max}$ increases. In Fig.SI. 2, this value is close to 3 and the total excess number of denatured bps does not exceed 3 on average. This is corroborated by the fact that the large θ torque is independent of r, mainly due to the few melted bps. In other words, even if r bp, or more, can in principle be melted to relax the bending stress, only a few of them actually do, since it costs more energy to melt more bases, whereas, owing to the small value of κ_B, a small denaturation bubble suffices to give the whole molecule a very small resistance to torque.

Note that N_r is essentially unchanged between the different fitted parameter sets discussed above, and ΔM_B varies by at most 20%, in the melted region only.

G. Bending-induced melting in 3D

The previous calculations can be extended in a straightforward way to the 3D case, with very similar qualitative conclusions. The physical meaning of the bending moment is less direct because of the axial symmetry ($m = 0$) imposed in the calculation of $p(\cos\theta)$. By contrast, the excess melting, ΔM_B, is meaningful for circular DNAs, where θ is close to 2π, with the reserves given above. The above argument now leads to $r_{\max} \approx 50$ bp. In Fig.SI. 3 one actually sees that for $r < 50$ bp, ΔM_B saturates at 10 bp near $\theta = \pi$. In the topical case where r is comparable to the chain persistence length (~ 150 bp), bending-induced melting of constrained DNA is expected to be virtually inexistent in 3D. As for large looped complexes, such as in Ref. [8] where $r \sim 1000$ bp, melting is not expected to stabilize or to facilitate looping either.

In contrast, non-linear behavior can play a significant role by making DNA much more flexible when the polymer is highly bent, such as in short circular DNA (see [7]) or in protein-DNA complexes. Our calculations on bending-induced melting, ΔM_B, give a good indication of the degree of melting following a sharp bending constraint. Note, however, that a complete treatment of cyclization would require imposing not only the angle θ but also the physical

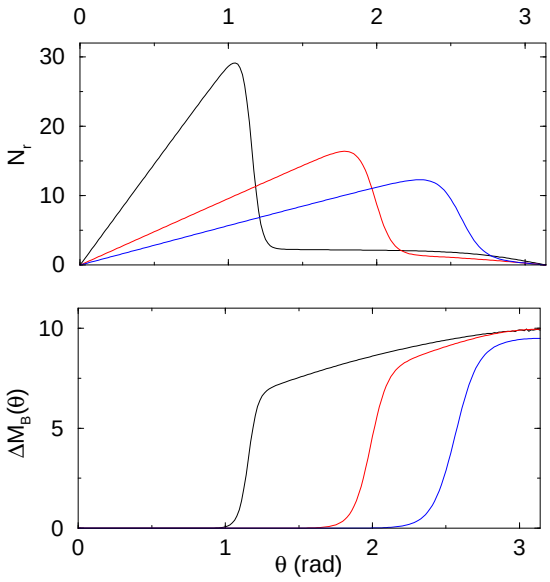

Fig.SI. 3: Torque N_r (top) and excess chain melting ΔM_B (bottom) as a function of θ, in 3D. Same parameter values as in Fig. 2A of the body of the text. From left to right, $r = 5, 15, 25$. The elasticity is linear until a threshold $\theta_c \propto \sqrt{r}$, where excessive bending induces bp melting.

distance between bps i and $i + r$ [9]. Although the full calculation is outside the scope of the present work, imposing θ does already contain some of the important physical features of cyclization. It is reasonable to expect that even for $\theta \simeq \pi$, our calculation reproduces the correct order of magnitude for cycled DNA. For instance, our 3D predictions concerning excess melting, e.g. $\Delta M_B \approx 10$ bp, could be checked by doing UV absorbance measurements on short circular DNAs.

[1] Palmeri, J., Manghi, M. & Destainville, N. Thermal denaturation of fluctuating finite DNA chains: The role of bending rigidity in bubble nucleation. *Phys. Rev. E* **77,** 011913 (2008).

[2] Abramowitch, M. & Stegun, I. A. *Handbook of Mathematical Functions with Formulas, Graphs and Mathematical Tables* (Wiley, New York, 1964).

[3] Palmeri, J., Manghi, M. & Destainville, N. Thermal denaturation of fluctuating DNA driven by bending entropy. *Phys. Rev. Lett.* **99,** 088103 (2007).

[4] Wiggins, P. A., *et al.* High flexibility of DNA on short length scales probed by atomic force microscopy. *Nature Nanotech.* **1,** 137-141 (2006).

[5] Wiggins, P. A. & Nelson, P. C. Generalized theory of semiflexible polymers. *Phys. Rev. E* **73,** 031906 (2006).

[6] Wiggins, P. A., Phillips, R. & Nelson, P. C. Exact theory of kinkable elastic polymers. *Phys. Rev. E* **71,** 021909 (2005).

[7] Lankas, F., Lavery, R. & Maddocks, J.H. Kinking occurs during molecular dynamics simulations of small DNA minicircles. *Structure* **14,** 1527-1534 (2006).

[8] Pouget, N., Turlan, C., Destainville, N., Salomé, L. & Chandler, M. IS*911* transpososome assembly as analysed by tethered particle motion. *Nucleic Acids Res.* **34,** 4313-4323 (2006).

[9] Yan, J. & Marko, J. F. Localized single-stranded bubble mechanism for cyclization of short double helix DNA. *Phys. Rev. Lett.* **93,** 108108 (2004).